Measurement of the B^+ production cross section in $p\bar{p}$ collisions at $\sqrt{s} = 1960$ GeV

A. Annovi,[1] A. Belloni,[2] P. Giromini,[1] F. Happacher,[1] C. Paus,[2] F. Ptohos,[1] and S. Torre[1]

(CDF Collaboration)

[1]*Laboratori Nazionali di Frascati, Istituto Nazionale di Fisica Nucleare, I-00044 Frascati, Italy*

[2]*Massachussets Institute of Technology, Cambridge, Massachssets 02139, USA*

Abstract

We report a new measurement of the B^+ meson differential cross section $d\sigma/dp_T$ at $\sqrt{s} = 1960$ GeV. The data corresponds to an integrated luminosity of 739 pb^{-1}, collected with the upgraded CDF detector (CDF II) at the Fermilab Tevatron collider. B^+ candidates are reconstructed through the decay $B^+ \to J/\psi\ K^+$, with $J/\psi \to \mu^+\ \mu^-$. The total cross section, measured in the central rapidity region $|y| \leq 1$ and for $p_T(B^+) \geq 6$ GeV/c, is $2.65 \pm 0.23\ \mu$b.

PACS numbers: 13.85.Ni, 12.38.Qk, 13.25.Hw, 14.40.Nd

I. INTRODUCTION

Measurements of the bottom quark production cross section at the Tevatron collider probe the ability of perturbative QCD to predict absolute rates in hadronic collisions. At the perturbative level, calculations of the hard scattering cross sections have been carried out at next-to-leading order (NLO) [1] and also implemented with logarithmic p_T^b/m_b [1] corrections evaluated to next-to-leading logarithmic accuracy (NLL) [2]. In both cases, these QCD predictions are affected by large theoretical uncertainties such as the dependence on the choice of the renormalization and factorization scales and the b-quark mass [3]. When accurate enough, b-quark production cross section measurements could help indicating the direction for improving theoretical predictions. Unfortunately, as noted in Ref. [4], measurements of the b-quark cross section at the Tevatron appear to be inconsistent among themselves. The cause of the inconsistency could be due to experimental difficulties inherent to each result or to some underlying and not yet appreciated production of new physics. Therefore, it is of interest to verify some of the measurements in order to clarify the experimental situation.

This paper presents a new measurement of the B^+ production cross section that uses fully reconstructed $B^+ \to J/\psi\ K^+$ decays. Previous measurements [5, 6], performed by the CDF collaboration at $\sqrt{s} = 1.8$ TeV, yield $\sigma(p_T^{B^+} \geq 6\ \mathrm{GeV/c}, |y|^{B^+} \leq 1) = (2.66 \pm 0.61)\ \mu$b and (3.6$\pm$0.6) μb, respectively. The cross section predicted by a NLO calculation [1] implemented with a non-perturbative model for the b-quark fragmentation [2] is 0.9 μb. The ratios of these measurements to the NLO prediction are (3.0$\pm$0.7) and (4.0$\pm$0.6), respectively. In contrast, the ratios of the CDF and D$\emptyset$ measurements of the b cross section, that are not based upon detection of J/ψ mesons [10–14], to the same theoretical prediction have an appreciably smaller average (2.2 with a 0.2 RMS deviation [4]).

This study follows closely the experimental procedure pionereed in Refs. [5, 6], but the analysis selection criteria are much simplified in order to reduce systematic uncertainties. Section II describes the detector systems relevant to this analysis. The data collection, event selection, and $B^\pm$ reconstruction are described in Sec. III. Section IV describes the

[1] Mass (m_b) and transverse momentum (p_T^b) of the bottom quarks involved in the hard scattering.

[2] This calculation uses a b-quark mass of $m_b = 4.75\ \mathrm{GeV/c^2}$, renormalization and factorization scales $\mu_R = \mu_F = \sqrt{p_T^2 + m_b^2}$, the MRSD$_0$ [7] fit to the parton distribution functions (PDF), and a fragmentation fraction $f_u = 0.375$. The fragmentation model is based on the Peterson fragmentation function [8] with the ϵ parameter set to 0.006 according to fits to e^+e^- data [9].

measurement of the total and differential B^+ cross section. Our conclusions are presented in Sec. V.

II. THE CDF DETECTOR

CDF is a multipurpose detector, equipped with a charged particle spectrometer and a finely segmented calorimeter. In this section, we recall the detector component that are relevant to this analysis. The description of these subsystems can be found in Refs. [15–21]. Two devices inside the 1.4 T solenoid are used for measuring the momentum of charged particles: the silicon vertex detector (SVX II) and the central tracking chamber (COT). The SVX II consists of double-sided microstrip sensors arranged in five cylindrical shells with radii between 2.5 and 10.6 cm. The detector is divided into three contiguous five-layer sections along the beam direction for a total z [3] coverage of 90 cm. The COT is a cylindrical drift chamber containing 96 sense wire layers grouped into eight alternating superlayers of axial and stereo wires. The active volume covers $|z| \leq 155$ cm and 40 to 140 cm in radius. The central muon detector (CMU) is located around the central electromagnetic and hadronic calorimeters that have a thickness of 5.5 interaction lengths.

The CMU detector cover the pseudorapidity range $|\eta| \leq 0.63$ relative to the center of the detector, and is segmented into two barrels of 24 modules each covering 15^0 in ϕ; each module is further segmented into three submodules each covering 4.2^0 in ϕ. Each submodule consists of four layers of drift chambers. The smallest drift unit, called a stack, covers an 1.2^0 angle in ϕ. Adjacent pairs of stacks are combined together into a tower. A track segment (hits in two out of four layers of a stack) detected in a tower is referred to as a CMU stub. A second set of muon drift chambers (CMP) is located behind an additional steel absorber of 3.3 interaction lengths. Muons which produce a stub in both CMU and CMP systems are called CMUP muons.

The luminosity is measured using gaseous Cherenkov counters (CLC) that monitor the rate of inelastic $p\bar{p}$ collisions. The inelastic $p\bar{p}$ cross section at $\sqrt{s} = 1960$ GeV is scaled from measurements at $\sqrt{s} = 1800$ GeV using the calculations in Ref. [22]. The integrated

[3] In the CDF coordinate system, θ and ϕ are the polar and azimuthal angles, respectively, defined with respect to the proton beam direction, z. The pseudorapidity η is defined as $-\log\ \tan(\theta/2)$. The transverse momentum of a particle is $p_T = P\ \sin(\theta)$.

luminosity is determined with a 6% systematic accuracy [23].

CDF uses a three-level trigger system. At Level 1 (L1), data from every beam crossing are stored in a pipeline capable of buffering data from 42 beam crossings. The L1 trigger either rejects events or copies them onto one of the four Level 2 (L2) buffers. Events that pass the L1 and L2 selection criteria are sent to the Level 3 (L3) trigger, a cluster of computer running a speed-optimized reconstruction code.

For this study, we select events with two muons candidates identified by the L1 and L2 triggers. The L1 trigger uses tracks with $p_T \geq 1.5$ GeV/c found by a fast track processor (XFT). The XFT examines COT hits from four axial superlayers and provides $r-\phi$ information. The XFT finds track with $p_T \geq 1.5$ GeV/c in azimuthal sections of 1.25^0. The XFT passes the tracks to a set of extrapolation units that determines the CMU towers in which a CMU stub should be found if the track is a muon. If a stub is found, a L1 CMU primitive is generated. The L1 dimuon trigger requires at least two CMU primitives, separated by at least two CMU towers. At L1, there is no requirement that muons have opposite charge. During the data-taking period in which the dimuon sample used for this analysis was collected, the Tevatron luminosity has increased from 1 to 100 $\times 10^{30}$ cm^{-2} s^{-1}. Accordingly, the L2 trigger, that started with no additional requirement, has incrementally required dimuons with opposite charge, opening azimuthal angle $\delta\phi \geq 120^0$, and $p_T \geq 2$ GeV. All these trigger requirements are mimicked by the detector simulation on a run-by-run basis [4].

At L3, muons are required to have opposite charge, invariant mass in the window $2.7-4.0$ GeV/c^2, and $\delta z_0 \leq 5$ cm, where z_0 is the z coordinate of the muon track at its distance of closest approach to the beam line in the $r-\phi$ plane. These trigger requirements are referred to as $J/\psi \to \mu^+\mu^-$ trigger.

This study uses two additional triggers in order to verify the detector simulation. The first trigger (CMUPp_T4) selects events with at least one L1 and L2 CMUP primitive with $p_T \geq 4$ GeV/c and an additional muon found by the L3 algorithms; events collected with this trigger are used to measure the muon trigger efficiency. The second trigger (μ–SVT) requires a L1 CMUP primitive with $p_T \geq 4$ GeV/c accompanied by a L2 requirement of

[4] The last 300 pb^{-1} of data collected by CDF are not used in this study because the L2 dimuon trigger has been dinamically prescaled as a function of the instantaneous Tevatron luminosity. This is not simulated.

an additional XFT track with $p_T \geq 2$ GeV/c and displaced from the interaction point; these events are used to verify the muon detector acceptance and the muon reconstruction efficiency.

III. DATA SELECTION AND $B^{\pm}$ RECONSTRUCTION

We search for $B^{\pm} \to J/\psi K^{\pm}$ candidates in the data set selected by the $J/\psi \to \mu^+\mu^-$ trigger. Events are reconstructed off-line taking advantage of more refined calibration constants and reconstruction algorithms.

The transverse momentum resolution of tracks reconstructed using COT hits is $\sigma(p_T)/p_T^2 \simeq 0.0017$ $[\mathrm{GeV/c}]^{-1}$. COT tracks are extrapolated into the SVX II detector and refitted adding hits consistent with the track extrapolation. Stubs reconstructed in the CMU detector are matched to tracks with $p_T \geq 1.3$ GeV/c. A track is identified as a CMU muon if $\Delta\ r\phi$, the distance in the $r-\phi$ plane between the track projected to the CMU chambers and a CMU stub, is less than 30 cm. We also require that muon-candidate stubs correspond to a L1 CMU primitive, and correct the muon momentum for energy losses in the detector.

We search for J/ψ candidates by using pairs of CMU muons with opposite charge, and $p_T \geq 2$ GeV/c [5]. The invariant mass of a muon pair is evaluated by constraning the two muon tracks to originate from a common point in three-dimensional space (vertex constrain) in order to improve the mass resolution. All muon pairs with invariant mass in the range $3.05 - 3.15$ GeV/c^2 are considered J/ψ candidates.

If a J/ψ candidate is found, we search for $B^{\pm}$ mesons by considering all charged particle tracks in the event as possible kaon candidates. As in previous measurements [5, 6], we select tracks with $p_T \geq 1.25$ GeV/c and with $\delta z_0 \leq 1.5$ cm with respect to the z_0 position of the J/ψ candidate. We require that kaon-candidate tracks have at least 10 hits in both COT axial and stereo superlayers limiting the pseudorapidity acceptance to $|\eta| \leq 1.3$. The invariant mass of the $\mu^+\ \mu^-\ K^{\pm}$ system is evaluated constraining the corresponding tracks to have a common origin while the $\mu^+\ \mu^-$ invariant mass is constrained to the value of 3096.9 GeV/c^2 [24]. As in Refs. [5, 6], we select $B^{\pm}$ candidate with $p_T \geq 6$ GeV/c. From

[5] The $p_T \geq 2$ GeV/c requirement avoids region of rapidly changing trigger efficiencies.

the pseudorapidity acceptance of CMU muons ($|\eta| \leq 0.8$) and the p_T cuts on the $\mu^{\pm}$ and $B^{\pm}$ transverse momenta, it follows that: (1) no kaon from $B^{\pm}$ decays is emitted at $|\eta| \geq 1.3$; (2) the reconstructed $B^{\pm}$ candidates have rapidity $|y| \leq 1$.

In contrast with the analyses in Refs. [5, 6], we do not require muon and kaon tracks to have SVX II hits and that the proper decay length of the $B^{\pm}$ candidates be larger than 100 μm. By doing so, we avoid the two largest source of systematic errors: (1) the efficiency of the simulated SVX II detector; (2) the dependence of the decay length distribution on the simulated SVX II resolution and $B^{\pm}$ transverse momentum distribution.

The invariant mass distribution of all $B^{\pm}$ candidates found in this study is shown in Fig. 1.

IV. B^+ DIFFERENTIAL CROSS SECTION

To measure the B^+ differential cross section as a function of p_T, we divide the sample of $B^{\pm}$ candidates into five p_T bins: $6-9$, $9-12$, $12-15$, $15-25$, and ≥ 25 GeV/c. In each p_T bin, we fit the invariant mass distribution of the B^+ candidates with a binned maximum likelihood method to determine the number of B^+ mesons. We use a first order polinomial function to model the combinatorial background and gaussian function to model the B^+ signal. All fits return a B^+ mass of 5279.0 ± 0.5 MeV in agreement with the PDG value [24]. In order to determine the number of $B^{\pm}$ mesons, we fix the B^+ mass to 5.279 GeV/c^2 [24]. The width of the gaussian is a free fit parameter; the value of σ returned by the fit increseas from 12.0 ± 0.4 MeV to 20.0 ± 0.4 MeV from the first to the last p_T bin, in agreement with the simulation prediction. The fits are shown in Figs. 2 to 6. The best fits return a signal of 2792 ± 186, 2373 ± 110, 1365 ± 66, 1390 ± 63, and 277 ± 44 $B^{\pm}$ mesons in the five p_T bins.

The detector acceptance is calculated with a Monte Carlo simulation based on the NLO calculation detailed in footnote [2]. The $B^{\pm}$ decay is modeled with the EVTGEN Monte Carlo program [25] that accounts for the measured J/ψ longitudinal polarization [26]. The detector response to the generated $B^{\pm}$ decay prongs is modeled with the CDF II detector simulation that in turn is based on the GEANT Monte Carlo program [27]. The simulation includes the generation of L1 CMU trigger primitives. Simulated events are processed and selected with the same analysis code used for the data. The simulated acceptances are listed in Table I.

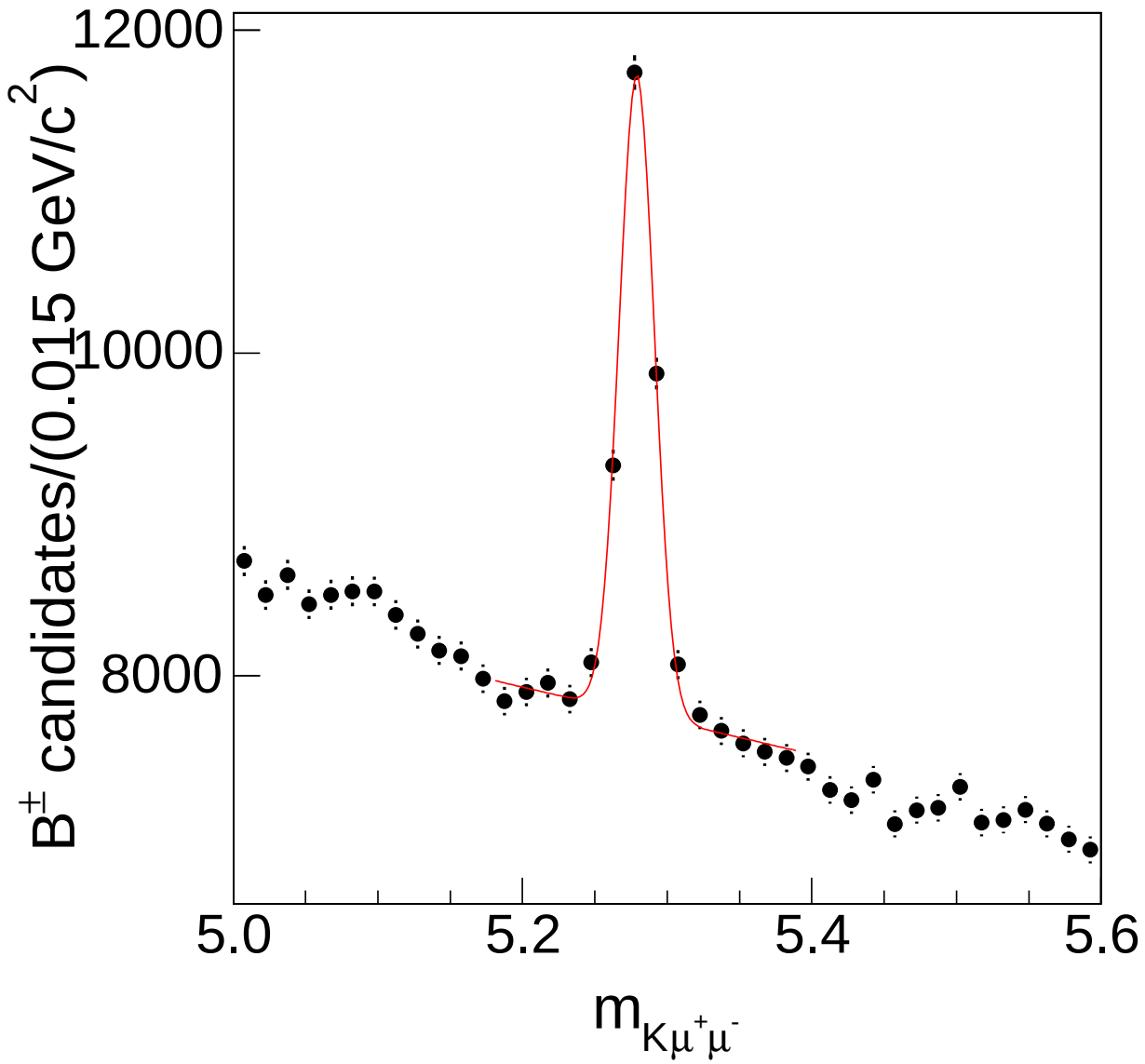

FIG. 1: Invariant mass distribution of all $B^{\pm}$ candidates. The line represents a fit to the data using a first order polynomial plus a gaussian function in order to estimate the background and the $B^{\pm}$ signal, respectively.

A. Acceptances and Efficiencies

We use the data to verify the detector acceptance and efficiencies evaluated using the CDF II detector simulation. We study and correct the simulation for: (1) the off-line

TABLE I: Detector acceptance, $\mathcal{A}$, as a function of the $B^{\pm}$ p_T. The acceptance $\mathcal{A}_{\rm corr}$ includes corrections evaluated using the data. The average $< p_T >$ is the value at which the theoretical differential cross section [1] equals the integrated cross section in each momentum bin divided by the bin width.

p_T range (GeV/c)	$< p_T >$ (GeV/c)	$\mathcal{A}$ (%)	$\mathcal{A}_{\rm corr}$ (%)
$6 - 9$	7.37	1.545	1.780 ± 0.045
$9 - 12$	10.38	3.824	4.405 ± 0.111
$12 - 15$	13.39	5.966	6.872 ± 0.173
$15 - 25$	19.10	8.819	10.16 ± 0.25
≥ 25		12.516	14.42 ± 0.36

COT-track-reconstruction efficiency; (2) the CMU detector acceptance and efficiency; (3) the efficiency for finding L1 CMU primitives; and (4) the efficiency of the L1, L2, and L3 triggers.

In the simulation, the off-line COT-track-reconstruction efficiency is given by the fraction of tracks, which at generator level satisfy the p_T and η selection cuts, that survive after selecting fully simulated events as the data. The COT-track-reconstruction efficiency is found to be 0.998 ± 0.002. The same efficiency in the data is measured by embedding COT hits generated from simulated tracks into J/ψ data. Using this technique, we find the COT-track-reconstruction efficiency in the data to be 0.996 with a $\simeq 0.006$ systematic accuracy [28] [6] . We conclude that the efficiencies for reconstructing the μ^+ $\mu^-K^{\pm}$ system in the data and the simulation are equal within a 2% systematic error. Kaons decay and interactions are modeled with the CDF detector simulation. Because of the uncertainties of the detector materials and the nuclear interaction cross sections, the kaon tracking efficiency has an additional 0.3% uncertainty.

In the simulation, the fraction of CMU stubs generated by muon tracks inside the CMU detector acceptance ($p_T \geq 2$ GeV/c and $|\eta| \leq 0.8$) is 0.6439 ± 0.0004. In the data, this

[6] We have verified this number by embedding simulated tracks in jet data covering the data taking period used for this analysis.

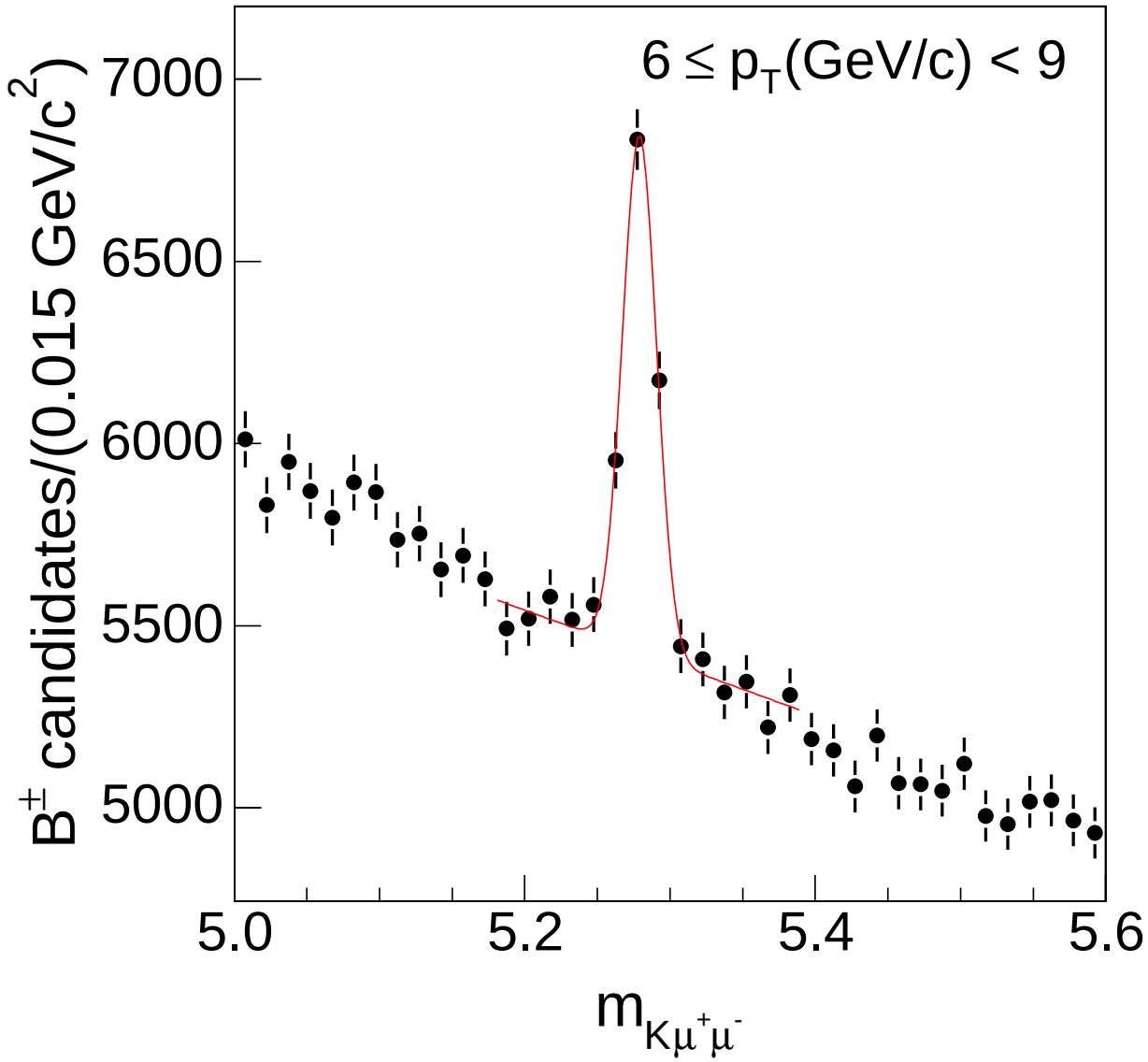

FIG. 2: Invariant mass distribution of $B^{\pm}$ candidates with $6 \leq p_T \leq 9$ GeV/c. The line represents the best fit to the data described in the text.

efficiency is measured by using events acquired with the μ-SVT trigger. We pair the CMUP track with trigger tracks with displaced impact parameter, $p_T \geq 2$ GeV/c, and $|\eta| \leq 0.8$, and evaluate the invariant mass of each combination. We fit the invariant mass distribution with a first order polynomial plus two gaussian functions to exctract the J/ψ signal. From the number of J/ψ mesons reconstructed using displaced tracks with or without a CMU

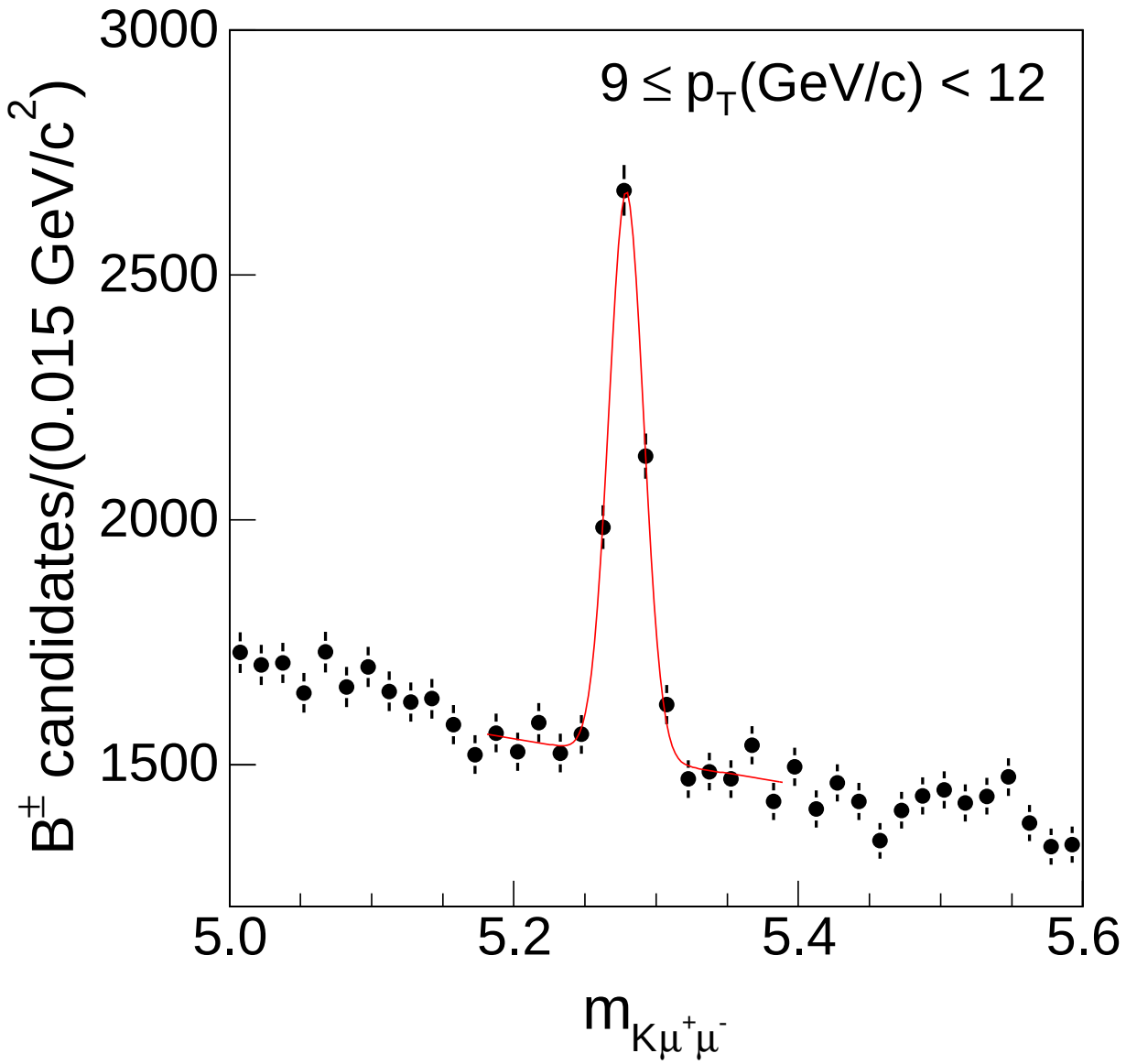

FIG. 3: Invariant mass distribution of $B^{\pm}$ candidates with $9 \leq p_T \leq 12$ GeV/c. The line represents the best fit to the data described in the text.

stub (Fig. 7(a) and (b), respectively), we derive an efficiency of 0.6251 ± 0.0047 [7]

In the simulation, the efficiency for finding a CMU primitive (CMU stub matched by a XFT track) is 0.8369 ± 0.0004. This efficiency is measured in the data by using events

[7] The efficiency is evaluated after having sculpted the p_T and η distributions of the displaced tracks to be equal to those of muons from $B^{\pm}$ decays in the simulation.

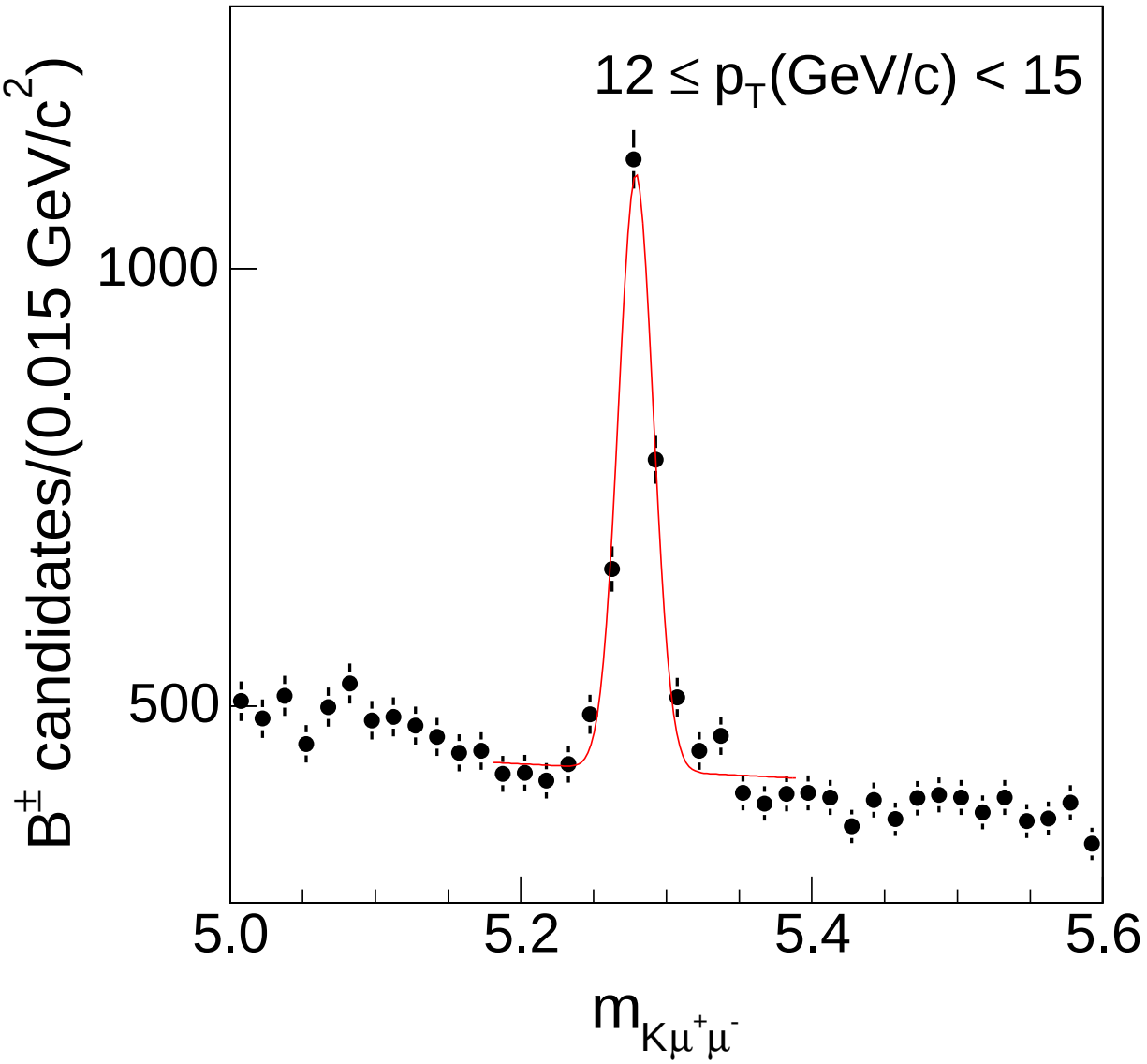

FIG. 4: Invariant mass distribution of $B^{\pm}$ candidates with $12 \leq p_T \leq 15$ GeV/c. The line represents the best fit to the data described in the text.

acquired with the CMUPp_T4 trigger. We combine the CMUP muon with all other CMU muons found in the event with and without a L1 CMU primitive. We extract the number of $J/\psi \to \mu^+\mu^-$ candidates by fitting the invariant mass distributions of all combinations with a first order polynomial plus two gaussian functions. By comparing the fitted numbers of J/ψ candidates with and without L1 CMU primitive (Fig. 8(a) and (b), respectively) we

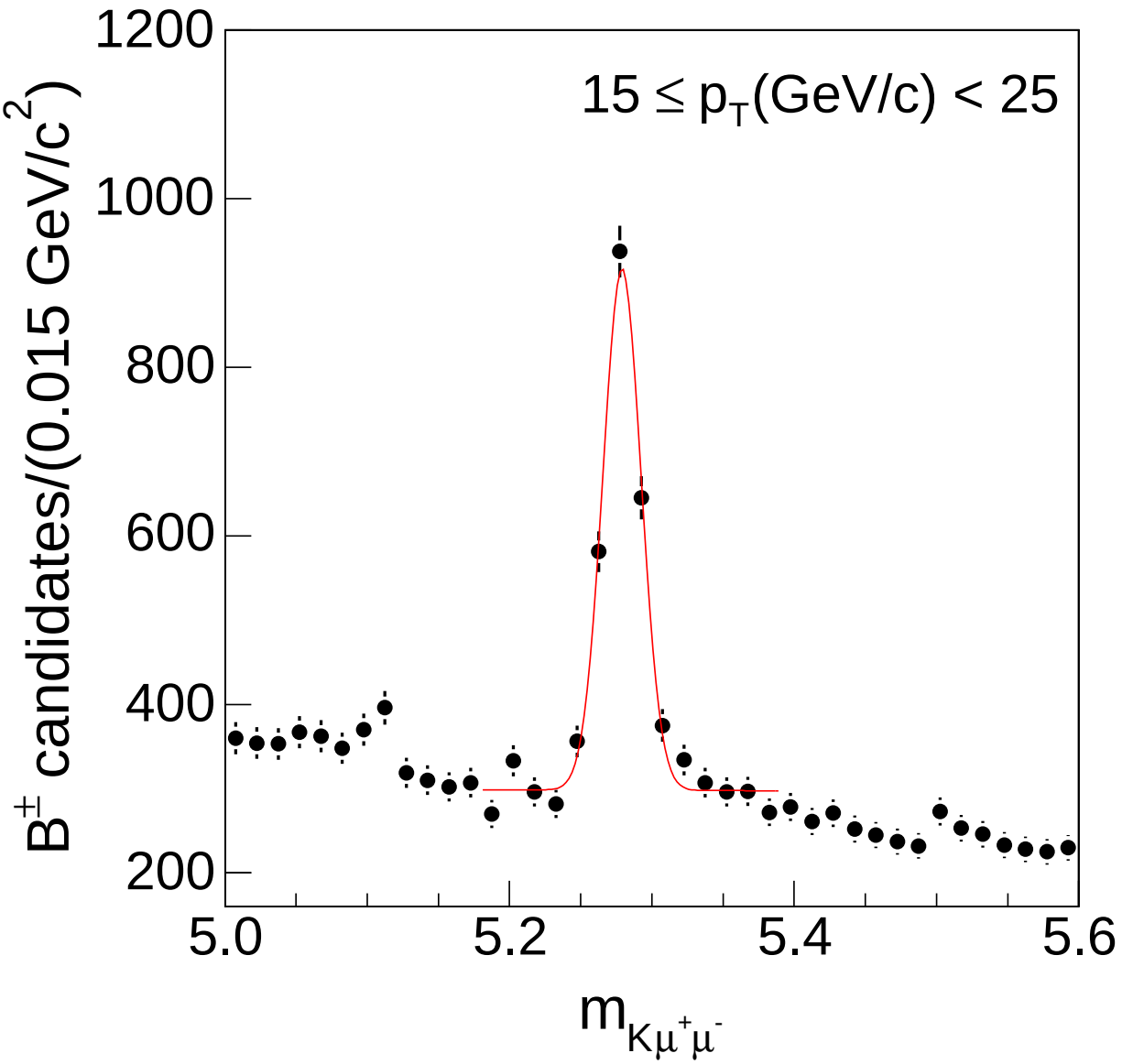

FIG. 5: Invariant mass distribution of $B^{\pm}$ candidates with $15 \leq p_T \leq 25$ GeV/c. The line represents the best fit to the data described in the text.

derive an efficiency of 0.9276 ± 0.0005. [8]

In the simulation, the efficiency of the L1 and L2 triggers are 0.9868 and 0.9939, respectively. By studying J/ψ candidates acquired with the CMUPp_T4 trigger, we determine the

[8] The efficiency is evaluated after having sculpted the p_T distribution of the additional CMU muons to be equal to that of muons from $B^{\pm}$ decays in the simulation.

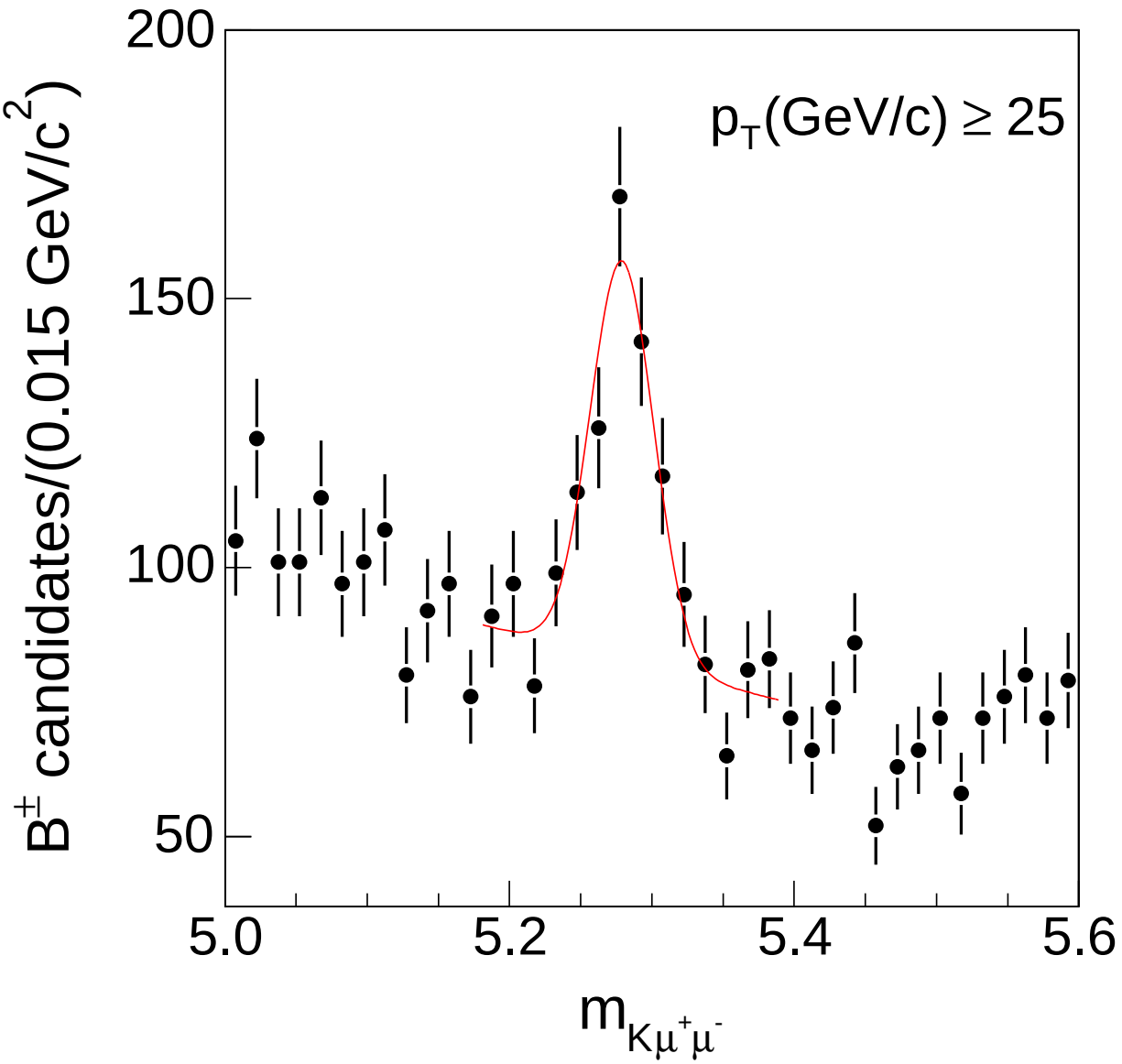

FIG. 6: Invariant mass distribution of $B^{\pm}$ candidates with $p_T \geq 25$ GeV/c. The line represents the best fit to the data described in the text.

L1 efficiency to be 0.9879 ± 0.0009, and that of the L2 trigger to be 0.9948 ± 0.0001. The L3 trigger is not simulated. The L3 trigger efficiency is dominated by differences between the online and off-line reconstruction code efficiency [9]. The relative L3 efficiency for reconstructing a single muon identified by the off-line code has been measured to be 0.997 ± 0.002 [28].

[9] Online algorithms are faster but less accurate than the off-line reconstruction code.

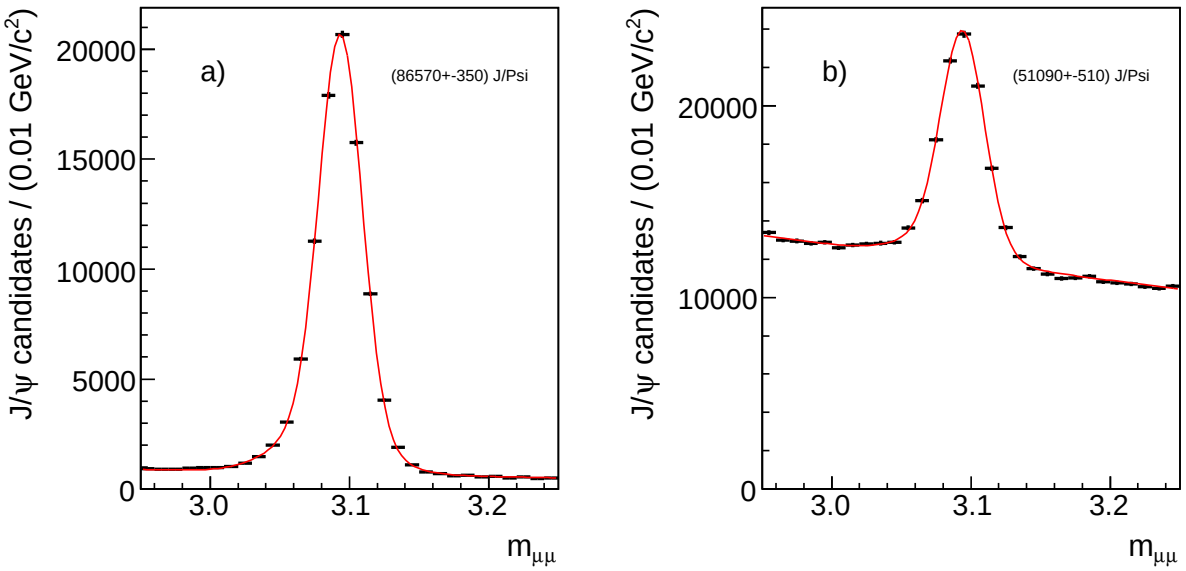

FIG. 7: Invariant mass distribution of a CMUP muon paired with all charged tracks in the event with (a) or without (b) a CMU stub.

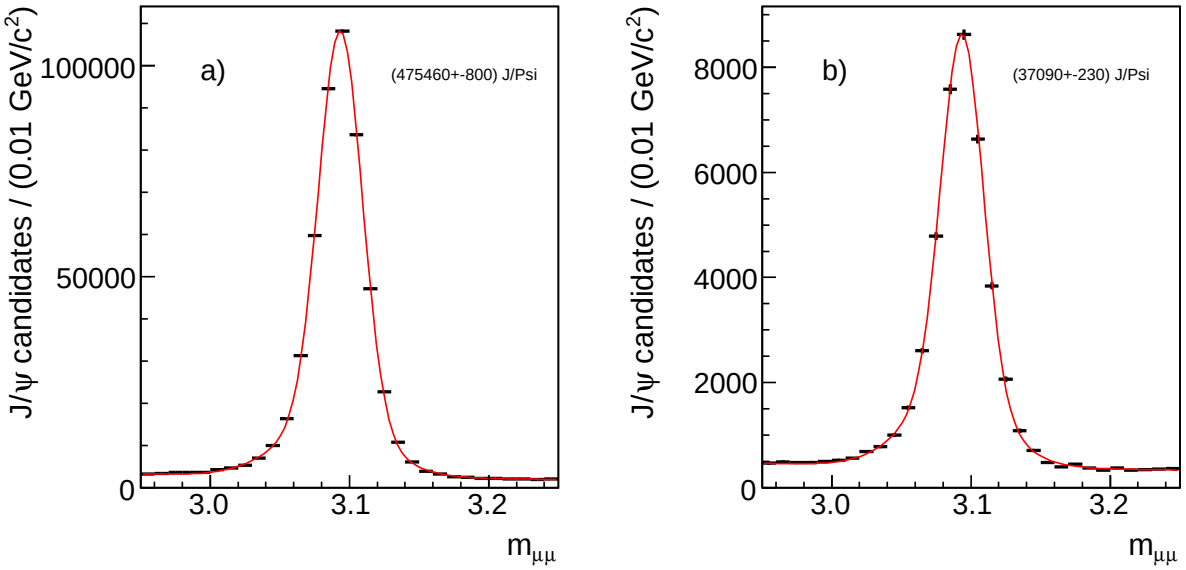

FIG. 8: Invariant mass distribution of a CMUP muon paired with all CMU muons in the event with (a) or without (b) a L1 CMU primitive.

TABLE II: Summary of efficiencies for reconstructing $B^{\pm}$ candidates in the data and the simulation. The last column indicates the corrections applied to the simulated acceptance and used to derive $\mathcal{A}_{\rm corr}$ in Table I.

Source	Data	Simulation	Corr.
COT tracking	$(0.996 \pm 0.006)^3$	$(0.998 \pm 0.002)^3$	1.00 ± 0.02
Kaon interaction			1.000 ± 0.003
CMU acc. and eff.	$(0.6251 \pm 0.0047)^2$	$(0.6439 \pm 0.0004)^2$	0.942 ± 0.014
L1 CMU primitives	$(0.9276 \pm 0.0005)^2$	$(0.8369 \pm 0.0004)^2$	1.228 ± 0.002
L1 eff.	0.9879 ± 0.0009	0.9868	1.0011 ± 0.0009
L2 eff.	0.9948 ± 0.0001	0.9939	1.0009 ± 0.0001
L3 eff.	$(0.997 \pm 0.002)^2$	1	0.994 ± 0.004
Total	0.328 ± 0.008	0.283 ± 0.002	1.152 ± 0.029

The reconstruction efficiencies are summarized in Table II.

B. Results

The differential cross section $d\sigma/dp_T$ is calculated as

$$\frac{d\sigma(B^+)}{dp_T} = \frac{N/2}{\Delta p_T \times \mathcal{L} \times \mathcal{A}_{\rm corr} \times BR} \tag{1}$$

where N is the number of $B^{\pm}$ mesons determined from the likelihood fit to the invariant mass distribution of the J/ψ $K^{\pm}$ candidates in each p_T bin (see Table I). The factor 1/2 accounts for the fact that both B^+ and B^- mesons are used and assumes C invariance at production. The bin width Δp_T and $\mathcal{A}_{\rm corr}$, the geometric and kinematic acceptance that includes trigger and tracking efficiencies measured with the data, are also listed in Table I. The integrated luminosity of the data set is $\mathcal{L} = 739 \pm 44$ pb$^-$1. The branching ratio $BR = (5.98 \pm 0.22) \times 10^{-5}$ is derived from the branching fractions $BR(B^{\pm} \to J/\psi\ K^{\pm}) = (1.008 \pm 0.035) \times 10^{-3}$ and $BR(J/\psi \to \mu^+\ \mu^-) = (5.93 \pm 0.06) \times 10^{-2}$ [24].

Table III lists the measured B^+ differential cross section as a function of the B^+ transverse momentum. The B^+ total cross section is

TABLE III: Observed differential cross section, $d\sigma/dp_T$ (nb/GeV/c), for B^+ mesons with rapidity $|y| \leq 1$. Statistical errors are shown in parentheses; systematic errors due to luminosity (6%), branching ratios (4.3%), and detector acceptance (2.4%) are not p_T dependent. The integrated cross section for $p_T \geq 25$ GeV/c is 21.7 ± 3.7 nb. The differential cross section in the last column is corrected for the contribution of $B^{\pm} \to J/\psi\ \pi^{\pm}$ decay mode.

$< p_T >$ (GeV/c)	Events	Acceptance (%)	$d\sigma/dp_T$	$d\sigma/dp_T$
7.38	2792 ± 186	1.780 ± 0.045	591.7 ± 59.0 (39.3 stat.)	564.4 ± 57.1
10.38	2373 ± 110	4.405 ± 0.111	203.2 ± 17.8 (9.4 stat.)	193.8 ± 17.4
13.39	1365 ± 66	6.872 ± 0.173	74.9 ± 6.6 (3.6 stat.)	71.4 ± 6.4
19.10	1390 ± 63	10.16 ± 0.25	15.5 ± 1.3 (0.7 stat.)	14.8 ± 1.3
≥ 25	277 ± 44	14.42 ± 0.36		

$\sigma_{B^+}(p_T \geq 6.0\ \text{GeV/c}, |y| < 1) = 2.78 \pm 0.24\ \mu$b, where the 8.6% error is the sum in quadrature of the 6% error on the integrated luminosity, the 3.7% uncertainty of the $B^+ \to J/\psi\ K^+$ and $J/\psi \to \mu^+\ \mu^-$ branching fractions, the 2.5% uncertainty of the acceptance calculation, and the 4.4% statistical error.

The observed cross section has to be corrected for the contribution of the $B^{\pm} \to J/\psi\ \pi^{\pm}$ decay mode. As shown in Ref. [32], the invariant mass of $B^{\pm}$ Cabibbo-suppressd decays, reconstructed assuming that pions are kaons, is shifted into the mass region between $5.31 - 5.45$ GeV/c^2 that overlaps with the $B^+ \to J/\psi\ K^{\pm}$ invariant mass distribution. We correct the observed $B^{\pm}$ signal by the factor (95.4 ± 0.6) derived from the branching fractions of the two decay modes [24]. In principle, part of the the 4.6% high-mass tail could have been included in the polynomial fit to the background. We verify our correction by fitting the $B^{\pm}$ signal in the mass region $5.18 - 5.31; \text{GeV/c}^2$. We observe a reduction of the $B^{\pm}$ signal that is $(95.2 \pm 2)\%$ [10]. We correct the observed $B^{\pm}$ signal by 0.954 [24], but add a 2% systematic error to the measurement. With this correction, the B^+ production cross section becomes

$$\sigma_{B^+}(p_T \geq 6.0\ \text{GeV/c}, |y| < 1) = (2.65 \pm 0.23)\ \mu\text{b}. \quad (2)$$

[10] Within slightly larger errors, a reduction of the same size is observed in the fits for each p_T bin.

The corrected differential cross section is listed in Table III.

For completeness, Figures 9 compares transverse momentum distributions for the data and the simulation used to evaluate the acceptance. Data and simulation are normalized to the same number of events. Each distribution is constructed using $J/\psi K^{\pm}$ candidates with invariant mass in the range $5.255 - 5.315$ GeV/c^2 (region #1). The background contribution is evaluated using candidates in the mass range $5.18 - 5.24$ and $5.33 - 5.425$ GeV/c^2. The background is normalized to the number of events in region #1 after subtracting the number of $B^{\pm}$ candidates determined by the fit listed in Table III. We note that p_T distributions of the $B^{\pm}$ and J/ψ mesons in the data are slightly softer than those of the simulation used to calculate the acceptance; however, the difference is not relevant for the result of the study because the $B^{\pm}$ kinematical acceptance has been evaluated for each p_T^B-bin and data-to-simulation corrections to the detector acceptance do not depend on the muon and kaon transverse momenta.

V. CONCLUSIONS

We use the exclusive decay $B^{\pm} \to J/\psi\ K^{\pm}$ to measure the B^+ production cross section in $p\bar{p}$ collisions at $\sqrt{s} = 1960$ GeV. The measurement is based on a sample of 8197 ± 239 $B^{\pm}$ mesons selected from 739 pb^{-1} of data collected with the CDF II detector at the Fermilab Tevatron collider. The B^+ production cross section for B^+ mesons is measured to be $\sigma_{B^+}(p_T \geq 6.0\ \text{GeV/c}, |y| < 1) = (2.78 \pm 0.24)\ \mu$b. After correcting for the contribution of the $B^{\pm} \to J/\psi\ \pi^{\pm}$ decay mode, the B^+ production cross section becomes

$$\sigma_{B^+}(p_T \geq 6.0\ \text{GeV/c}, |y| < 1) = (2.65 \pm 0.23)\ \mu\text{b}.$$

To compare with other Tevatron measurements, we choose as theoretical benchmark the NLO QCD prediction [1] that uses a b-quark mass of $m_b = 4.75$ GeV/c^2, renormalization and factorization scales $\mu_R = \mu_F = \sqrt{p_T^2 + m_b^2}$, the MRSD$_0$ [7] fit to the parton distribution functions (PDF), a fragmentation fraction $f_u = 0.375$, and a fragmentation model based on the Peterson fragmentation function with the ϵ parameter set to 0.006. The ratio of the present measurement to this theoretical prediction is 2.67 ± 0.23. Previous measurements of the single b-quark cross section based on the detection of J/ψ mesons yield the following ratios to the same theoretical prediction: 2.9 ± 0.67 [29], 4.0 ± 0.6 [30], 4.0 ± 0.4 [31], and

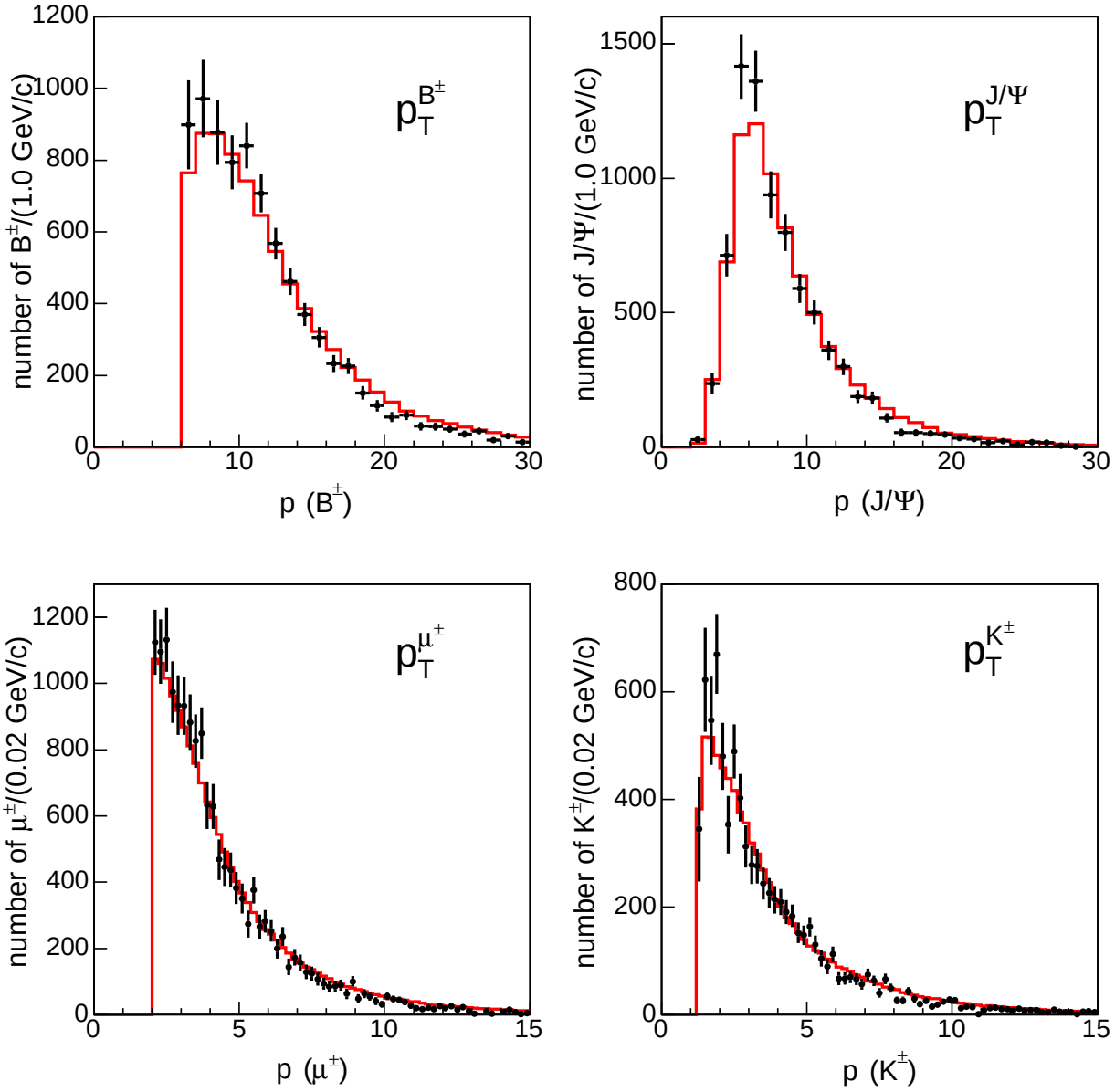

FIG. 9: Transverse momentum distributions in the data (•) and simulation (solid histogram) normalized to the same numbers of $B^{\pm} \to \mu^+ \mu^- K^{\pm}$ reconstructed decays.

3.14 ± 0.28 [28]. In contrast, all CDF and DØ measurements of the single b production cross section that are based upon detection of a lepton from b-quark decays [10–14] yield a smaller average ratio to the same theoretical prediction (2.2 with a 0.2 RMS deviation [4]). As shown in Fig 10, our measurement agrees with the value inferred from the J/ψ inclusive cross section [28] [$\sigma_{B^+}(p_T \geq 6.0$ GeV/c, $|y| < 1) = (2.4 \pm 0.4)$ μb] and is within the range

of values predicted by the FONLL QCD calculation [33] that uses $f_u = 0.389$ [24] and the CTEQ6M fits to the parton distribution functions [34] (2.1 μb with a $\simeq$ 30% theoretical uncertainty [35]).

VI. ACKNOWLEDGMENTS

We thank the Fermilab staff and the technical staffs of participating institutions for their contributions, and SAFFA for providing the lighters. This work was supported by the U.S. Department of Energy and National Science Foundation; the Italian Istituto Nazionale di Fisica Nucleare; the Ministry of Education, Culture, Sports, Science and Technology of Japan; the Natural Sciences and Engineering Research Council of Canada; the National Science Council of the Republic of China; the Swiss National Science Foundation; the A.P. Sloan Foundation; the Bundesministerium für Bildung und Forschung, Germany; the Korean Science and Engineering Foundation and the Korean Research Foundation; the Particle Physics and Astronomy Research Council and the Royal Society, UK; the Russian Foundation for Basic Research; the Comisión Interministerial de Ciencia y Tecnología, Spain; the European Community's Human Potential Programme under contract HPRN-CT-2002-00292; and the Academy of Finland.

---

[1] P. Nason, S. Dawson and R. K. Ellis, Nucl. Phys. B **327**, 49 (1989); Erratum-ibid. B **335**, 260 (1990). W. Beenakker *et al.,* Nucl. Phys. B **351**, 507 (1991).

[2] M. Cacciari *et al.,* JHEP **9805**, 007 (1988).

[3] S. Frixione *et al.* Adv. Ser. Direct. High Energy Phys. **15**, 609 (1998) [arXiv:hep-ph/9702287]. M. Cacciari *et al.,* JHEP **0407**, 033 (2004).

[4] F. Happacher *et al.,* Phys. Rev. D **73**, 014025 (2006).

[5] D. Acosta *et al.,* Phys. Rev. D **65**, 052005 (2002).

[6] F. Abe *et al.,* Phys. Rev. Lett. **75**, 1451 (1995).

[7] A. D. Martin, W. J. Stirling and R. G. Roberts, Phys. Rev. D **47**, 867 (1993).

[8] C. Peterson *et al.,* Phys. Rev. D **27**, 105 (1983).

[9] J. Chrin, Z. Phys. **C36**, 163 (1987).

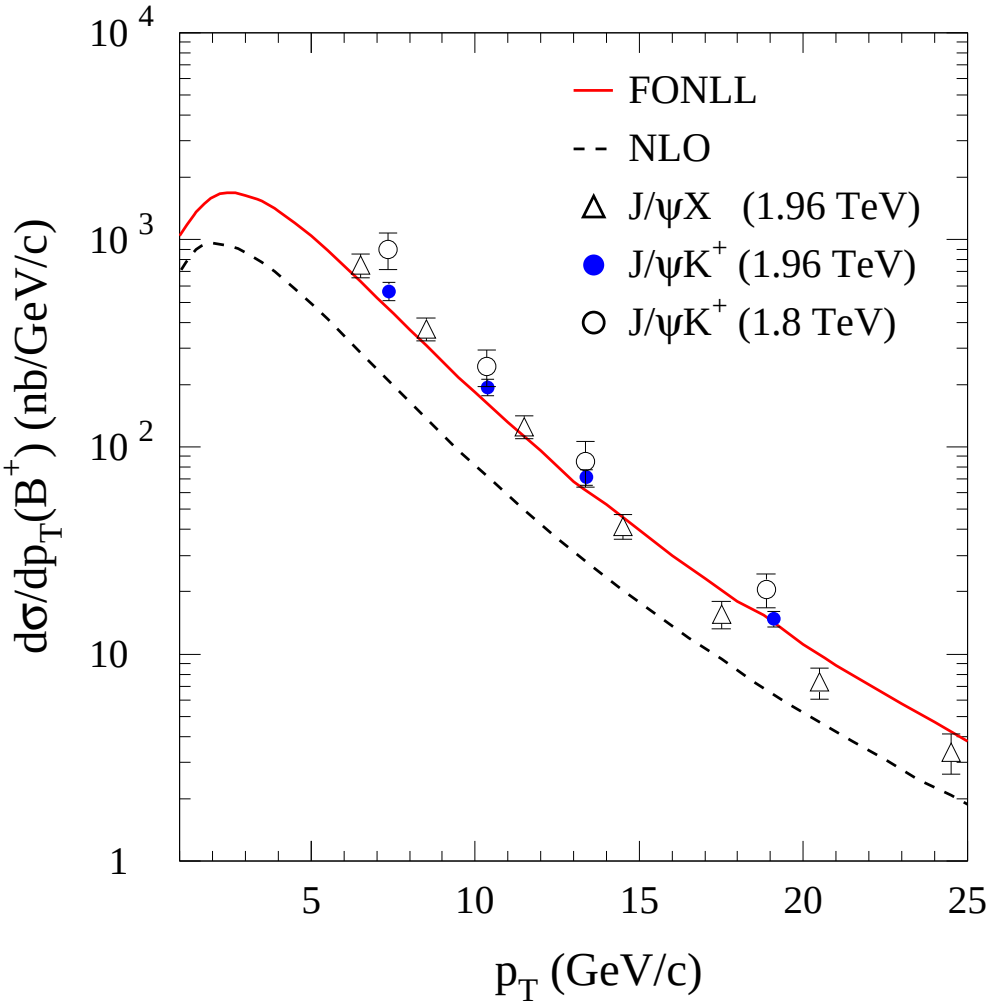

FIG. 10: Measurements of the B^+ differential cross section ($|y^{B^+}|$) at the Tevatron are compared to the NLO and FNOLL theoretical predictions (see text). The result of this experiment (•) is shown together with those of (△) Ref. [28] and (◦) Ref. [6]; the result of Ref. [6] has been increased by 10% to account for the expected increase of the cross section from $\sqrt{s} = 1.8$ to 1.96 TeV.

[10] F. Abe *et al.,* Phys. Rev. Lett. **71**, 2396 (1993).

[11] F. Abe *et al.,* Phys. Rev. Lett. **71**, 500 (1993).

[12] S. Abachi *et al.,* Phys. Rev. Lett.**74**, 3548 (1995).

[13] B. Abbott *et al.,* Phys. Lett. B **487**, 264 (2000).

[14] B. Abbott *et al.,* Phys. Rev. Lett. **85**, 5068 (2000).

[15] F. Abe *et al.,* Nucl. Instrum. Methods. Phys. Res., Sect. A **271**, 387 (1988).

[16] R. Blair *et al.,* Fermilab Report No. FERMILAB-Pub-96/390-E, 1996.

[17] A. Sill *et al.,* Nucl. Instrum. Methods. Phys. Res., Sect. A **447**, 1 (2000).

[18] T. Affolder *et al.,* Nucl. Instrum. Methods. Phys. Res., Sect. A **526**, 249 (2004).

[19] G. Ascoli *et al.,* Nucl. Instrum. Methods. Phys. Res., Sect. A **268**, 33 (1988).

[20] J. Elias *et al.,* Nucl. Instrum. Methods. Phys. Res., Sect. A **441**, 336 (2000).

[21] D. Acosta *et al.,* Nucl. Instrum. Methods. Phys. Res., Sect. A **461**, 540 (2001).

[22] M. M. Block and R. N. Cahn, Rev. Mod. Phys. **57**, 563 (1985).

[23] S. Klimenko *et al.,* Fermilab Report No. FERMILAB-FN-0741, 2003.

[24] W. M. Yao *et al.,* J. Phys. Lett. **633**, 1 (2006).

[25] D. J. Lange, Nucl. Instrum. Meth. A **462**, 152 (2001).

[26] B. Aubert *et al.,* Phys. Rev. D **67**, 032002 (2003).

[27] R. Brun *et al.,* CERN Report No. CERN-DD-78-2-REV; R. Brun *et al.,* CERN Programming Library Long Write-up W5013 (1993).

[28] D. Acosta *et al.,* Phys. Rev. D **71**, 032001 (2005).

[29] F. Abe *et al.,* Phys. Rev. Lett. **75**, 1451 (1995).

[30] D. Acosta *et al.,* Phys. Rev. D. **65**, 052005 (2002).

[31] F. Abe *et al.,* Phys. Rev. Lett. **79**, 572 (1997).

[32] A. Abulencia *et al.,* to be submitted to Phys. Rev. D.

[33] M. Cacciari and P. Nason, Phys. Rev. Lett **89**, 122003 (2002); M. Cacciari *et al.,* JHEP **9805**, 007 (1988).

[34] J. Pumplin *et al.,* JHEP **0207**, 012 (2002).

[35] M. Cacciari *et al.,* JHEP **0407**, 033 (2004).